Electronic Supplementary Material (ESI) for Journal of Materials Chemistry A.
This journal is © The Royal Society of Chemistry 2019

Electronic Supplementary Material (ESI) for Journal of Materials Chemistry A.
This journal is © The Royal Society of Chemistry 2019

Supporting Information

g-C_3N_4 Templated Synthesis of Fe_3C@NSC Electrocatalyst Enriched with Fe-N_x Active Sites for Efficient Oxygen Reduction Reaction

Ahmed A. Eissa,[ab] Shaik Gouse Peera,[a] Nam Hoon Kim[a] and Joong Hee Lee [ac]*

[a] Advanced Materials Institute of BIN Convergence Technology (BK21 Plus Global Program) & Department of BIN Convergence Technology, Chonbuk National University, Jeonju, Jeonbuk 54896, Republic of Korea. E-mail: jhl@chonbuk.ac.kr

[b] Department of Chemistry, South Valley University, Qena, 83523, Egypt

[c] Carbon Composite Research Centre, Department of Polymer-Nano Science and Technology, Chonbuk National University, Jeonju, Jeonbuk 54896, Republic of Korea

Experimental Section

1) Chemicals

All chemicals were utilized as received in all experiments without any further purification. Ferric nitrate nonahydrate ($Fe(NO_3)_3.9H_2O$, ≥99.95% purity), dicyandiamide ($C_2H_4N_4$, 99.0% purity) , thiourea (CH_4N_2S, ≥99.0% purity), glucose ($C_6H_{12}O_6$, ≥99.5% purity), potassium thiocyanate (KSCN, ≥99.0% purity), perchloric acid ($HClO_4$, 70 wt.%), potassium hydroxide (KOH, ≥85% purity), ethanol (C_2H_5OH, ≥99.8% purity), methanol (CH_3OH, ≥99.9% purity), Nafion solution (5 wt.%), and commercially carbon–supported platinum (Pt/C, 20 wt.%) were purchased from Sigma–Aldrich. Argon, nitrogen, and oxygen gases were provided in cylinders by SIAD Macchine Impianti company with 99.99% purity. Ultrapure deionized water (>18 MΩ cm resistivity) obtained from a Milli–pore Milli-Q system was used for the preparation of all aqueous solutions.

2) Synthesis of the catalysts

$Fe(NO_3)_3.9H_2O$, CH_4N_2S, $C_6H_{12}O_6$ and $C_2H_4N_4$ were mixed together with 1:1:1:4 wt. ratio, respectively, then uniformly ground into fine powder using a mortar with pestle for 20 min without adding any solvent. The mixture was allowed to completely dry at room temperature. The resulting homogeneous mixture was put into an alumina combustion boat, then the boat was placed at the center of a horizontal quartz tube furnace and subjected to a temperature-programmed reaction. The mixture was initially heated under argon atmosphere at 550 °C for 2 h at heating rate of 3 °C min^{-1} then calcined at 900 °C for 2 h, at heating rate of 5 °C min^{-1}. In this process, dicyandiamide would be thermally converted into graphitic carbon nitride ($g–C_3N_4$) at 550 °C. Figure S1 (Supporting Information) displays the temperature program applied to synthesize the electrocatalyst. After completing the pyrolysis reaction and cooling down, the obtained black material was ground into fine powder, then subjected to an acid leaching process with sulfuric acid (1.0 M) for 4 h at 80 °C. The acid-treated sample was washed several times with ultrapure water until neutral solution was obtained, then dried overnight at 70 °C in a vacuum oven. For comparative studies and to attain more knowledge about structure-electrocatalytic performance relationships, the following additional samples were considered: (1) three samples were synthesized by keeping the same precursor ratio at 1:1:1:4 but the temperature was changed to 700, 800 or 1000 □C, to investigate the influence of pyrolysis temperature on the catalyst performance, (2) Four samples without Fe precursor, DCDA, glucose, or thiourea were synthesized to demonstrate the synergistic effect of the precursors on promoting the catalytic performance of the electrocatalyst toward the ORR, (3) two samples were prepared at 900 ^{o}C but the weight ratio of iron salt with respect to the other precursors [($Fe(NO_3)_3.9H_2O$:CH_4N_2S:$C_6H_{12}O_6$:$C_2H_4N_4$) was altered to **0.4**:1:1:4 and **1.6**:1:1:4

3) Physical characterization

The crystalline properties and nature of phases existed in the prepared samples were investigated by powder X–ray diffraction (PXRD) using a diffractometer (Rigaku corporation, D/Max 2500V/PC, Tokyo, Japan) with Cu–Kα radiation (λ = 0.154 nm) in the 2θ range from 10 to 90° at scanning rate of 2° min^{-1}. Raman spectroscopy of the catalysts were recorded at room temperature in the spectral range of 500–3500 cm^{-1} using a Raman Imaging Microscope at 532 nm excitation laser (Tokyo Instruments Co., Nanofinder 30, Japan). Thermogravimetric analysis (TGA) was performed from room temperature to 900 °C under air atmosphere using a Q50 (TA Instrument, USA) at heating rate of 5 °C min^{-1} to estimate the total content of iron in the as-synthesized materials. Scanning electron microscopy (SEM) images were taken to examine the morphological features of the synthesized materials using a field emission SEM (FE-SEM; SUPRA 40 VP; Carl Zeiss, Germany) located in the Center for University–Wide Research Facilities (CURF), Chonbuk National University, South Korea. Transmission electron microscopy (TEM), scanning TEM (STEM) and high resolution TEM (HRTEM) were carried out by JEM–2200FS instrument (JEOL Co., USA) operated at working voltage of 200 kV, located at the Jeonju Center of the Korea Basic Science Institute (KBSI). The samples were prepared for imaging by dispersing the catalyst powder in ultrahigh–pure ethanol, then dropping the dilute ethanolic-suspension solution of the catalyst onto a carbon microgrid corroborative by a 300-mesh copper grid. Nitrogen adsorption–desorption isotherms were recorded at 77 K by Micromeritics ASAP 2020 instrument. All samples were degassed at 200 °C under vacuum for 6 h before nitrogen physisorption measurements. The specific surface areas were measured by the Brunauer–Emmett–Teller (BET) method. The average pore size distribution (PSD) curves were calculated with the Barrett–Joyner–Halenda (BJH) method, based on the analysis of the desorption branch of the isotherm. The total pore volume was estimated from the quantity of adsorbed nitrogen at a relative pressure of 0.99. X–ray photoelectron spectroscopy (XPS) was utilized for the elemental identification and determining the relative composition of the constituents in the surface region of the synthesized materials by using Theta Probe AR–XPS System (Thermo Fisher Scientific, UK) with a monochromatic X–ray source (Al $K\alpha^+$) located at the Korea Basic Science Institute (KBSI, Busan).

4) Electrochemical measurements

4.1. Electrochemical evaluation

All the electrochemical measurements were performed in a conventional three-electrode cell using an electrochemical workstation machine (CH660E Instruments, Inc., USA) equipped with a glassy carbon rotating disk electrode (RDE) at room temperature (298 *K*). A platinum wire and Ag/AgCl saturated KCl were employed as counter and reference electrodes, respectively. Glassy carbon (GC) electrode (3.0 mm diameter, 0.0706 cm^2, PINE Instrument Inc.) was utilized as a working electrode for cyclic voltammetry (CV) and RDE measurements. Before dropping the catalyst ink on the electrode surface, GC electrode was polished with alumina powders having an average size of 0.5, 0.15, and 0.05 μm (CH Instrument Inc.) successively, to remove any impurities on the electrode surface, then rinsed with ultrapure water and ethanol to eliminate the alumina powder.

4.2. Preparation of the electrodes

Suspensions of the as-synthesized electrocatalysts were prepared by dispersing 10.0 mg of the catalyst in 1.0 ml solution containing 295 μl of ethanol, 695 μl of deionized water followed by ultrasonication for 30 min. Thereafter, 10 μl of 0.5wt.% Nafion were added to the previous mixture to enhance the dispersion of the catalyst suspension and improve the binding with the GC electrode surface, then the mixture was ultrasonicated again for a certain time until getting a homogeneous suspension. The ink of the commercially carbon-supported platinum (Pt/C, 20 wt.%) was prepared according to the above procedure but with dispersing 5.0 mg of Pt/C powder in 1.0 ml solution. Posteriorly, a certain amount of the as-prepared ink was dropped onto GC electrode surface, then dried in air at room temperature resulting in a loading of 400 μg cm^{-2} for Fe_3C@NSC electrocatalysts and 250 μg cm^{-2} for Pt/C (50 μg_{Pt} cm^{-2}).

4.3. Cyclic voltammetry measurements

The CV experiments were done either in 0.1 M KOH electrolyte in the potential window from −0.80 to 0.20 V or in 0.1 M $HClO_4$ electrolyte in the potential window from −0.20 to +0.80 V vs saturated Ag/AgCl reference electrode at a scanning rate of 50 mV s^{-1} using the CH660E machine. Prior to CV tests, the electrolyte solution was bubbled with the high-purity nitrogen or oxygen for 30 min with a flowing rate of 100 ml/min to ensure a complete saturation with gases. A flow of O_2 was continuously maintained over the electrolyte during the record of the CVs curves. Before testing the electrocatalytic performance, the working electrode was cycled for 100 cycles at scan rate of 50 mV s^{-1} in N_2-saturated 0.10 M KOH or 0.10 M $HClO_4$ solution, then cycled again for another 100 cycles at the same scan rate in the O_2-saturated electrolytes to obtain stable and reproducible signals.

4.4. Rotating disk electrode (RDE) polarization curves

The RDE experiments were implemented in O_2-saturated 0.1 M KOH, or in O_2-saturated 0.1 M $HClO_4$ electrolytes at different rotation speeds from 400 to 2800 rpm at a sweep rate of 5 mV s^{-1}, to study the ORR performance for the prepared materials. All currents were corrected for the background current measured in N_2-saturated electrolyte. The current densities were normalized by the geometric surface area of the glassy carbon electrode. The onset potential was defined as the potential at which the current density exceeded a threshold value of 0.1 mA cm^{-2} meanwhile the half–wave potential ($E_{1/2}$) is the potential which corresponds to 50% of the diffusion–limiting current density. The number of electrons transferred (*n*) was calculated from the slopes of the fitted linear curves based on the detailed analysis the Koutecky–Levich (K–L) equation at different electrode potentials, where the relation between $J^{-1}$and $\omega^{-1/2}$ was plotted:

$$\frac{1}{J}=\frac{1}{J_K}+\frac{1}{J_L}=\frac{1}{J_K}+\frac{1}{B\omega^{1/2}}$$

$$B=0.62nFC_{O_2}(D_{O_2})^{2/3}v^{-1/6}$$

$$J_K=nFkC_{O_2}$$

Where, J is the measured current density at a specific potential, J_K is the kinetic current density, J_L is the diffusion–limiting current density , ω is the electrode angular rotation speed in rad/s ($\omega = 2\pi N$, N is the linear rotation speed), B is related to diffusional current density, and can be calculated from the slopes of the K–L plots based on the K–L equation (B is the reciprocal of slope), n represents the number of electrons transferred per oxygen (O_2) molecule, F is the Faraday constant (F = 96485 C mol^{-1}), C_{O_2} is the bulk concentration of O_2 (1.20×10^{-3} mol L^{-1} for 0.10 M KOH aqueous solution and 1.26×10^{-3} mol L^{-1} for 0.10 M $HClO_4$ aqueous solution), D_{O_2} is the diffusion coefficient of O_2 (1.90×10^{-5} cm^2 s^{-1} for 0.10 M KOH solution and 1.93×10^{-5} cm^2 s^{-1} for 0.10 M $HClO_4$ solution), and v is the kinematic viscosity of the electrolyte (0.01 cm^2 s^{-1} for both 0.10 M KOH and 0.10 M $HClO_4$ aqueous solutions). The coefficient 0.62 is indicated as the conversion factor for the rotation velocity expressed in revolutions per minute (rpm). The mass activity was estimated via the normalization of J_K with the catalyst mass. In the Tafel plots (E v*s* log J_k), the kinetic current density was determined from the mass-transport correction of RDE based on the K–L equation:

$$J_K=\frac{J\times J_L}{J_L-J}$$

4.5. Durability and methanol cross over tests

The long–term accelerated stability tests for the optimized electrocatalyst and Pt/C were done in O_2-saturated 0.10 M KOH and 0.10 M $HClO_4$ electrolyte, by the potential cycling of the working electrode from 0.60 to 1.2 V and from 0.50 to 1.1 V vs RHE, respectively for a continuous 12 000 potential cycles at a scan rate of 50 mV s^{-1} that can provide harsh degradation conditions. After finishing the cyclic stability test, the active material loaded on the working electrode was undergone to the polarization tests, and the variations in the onset potential and half–wave potential ($E_{1/2}$) before and after 12 000 cycles were determined. In addition, the durability test was evaluated by the chronoamperometric test for 30 h and 20 h at 0.60 V vs RHE in O_2-saturated 0.10 M KOH and O_2-saturated $HClO_4$ solution, respectively, at a rotation rate of 1600 rpm. The methanol tolerances of the electrocatalyst and Pt/C were evaluated by chronoamperometry. The chronoamperometric responses were carried out for 5000 s at 0.60 V vs RHE and rotation speed of 1600 rpm.

Potential conversion

All the potentials were measured vs saturated Ag/AgCl reference electrode then converted to the reversible hydrogen electrode (RHE) scale using Nernst equation:

$$E_{\mathrm{RHE}} = E_{\mathrm{Ag/AgCl}} + 0.059\mathrm{pH} + E^{\circ}_{\mathrm{Ag/AgCl}}$$

where E_{RHE} is the converted potential vs RHE, $E_{\mathrm{Ag/AgCl}}$ is the experimental potential calculated against the Ag/AgCl reference electrode, and $E^{\circ}_{\mathrm{Ag/AgCl}}$ is the standard potential of the saturated Ag/AgCl at 25 °C (0.197 V).

Calculating the electrochemical accessible (active) surface area (EASA)

The electrochemical active surface area (EASA) of Fe_3C@NSC and Pt/C (20%) were determined form the electrochemical double-layer capacitance (C_{dl}) of the catalytic surface (*J. Am. Chem. Soc*. **2015**, 137, 4347). For calculating the C_{dl}, the potential was scanned at various scan rates of 5, 10, 25, 50, 75, and 100 mV s^{-1}, in the non-Faradic region (1.065 to 1.145 V vs RHE) (Fig. S20a,b†), where no electrochemical features of faradic current were noticed in this region. The current (mA) in both anodic and cathodic regions of the cyclic voltammetry curve was then plotted vs scan rate, where straight lines were obtained whose slope was assigned to C_{dl} (Fig. S20c,d†). The EASA was calculated by dividing the C_{dl} by specific capacitance (C_s). The Cs in 0.10 M KOH lies between 25 to 35 µF, hence we used the average value of 30 µF (*Adv. Funct. Mater.* **2016**, *26*, 2150), in the herein calculations.

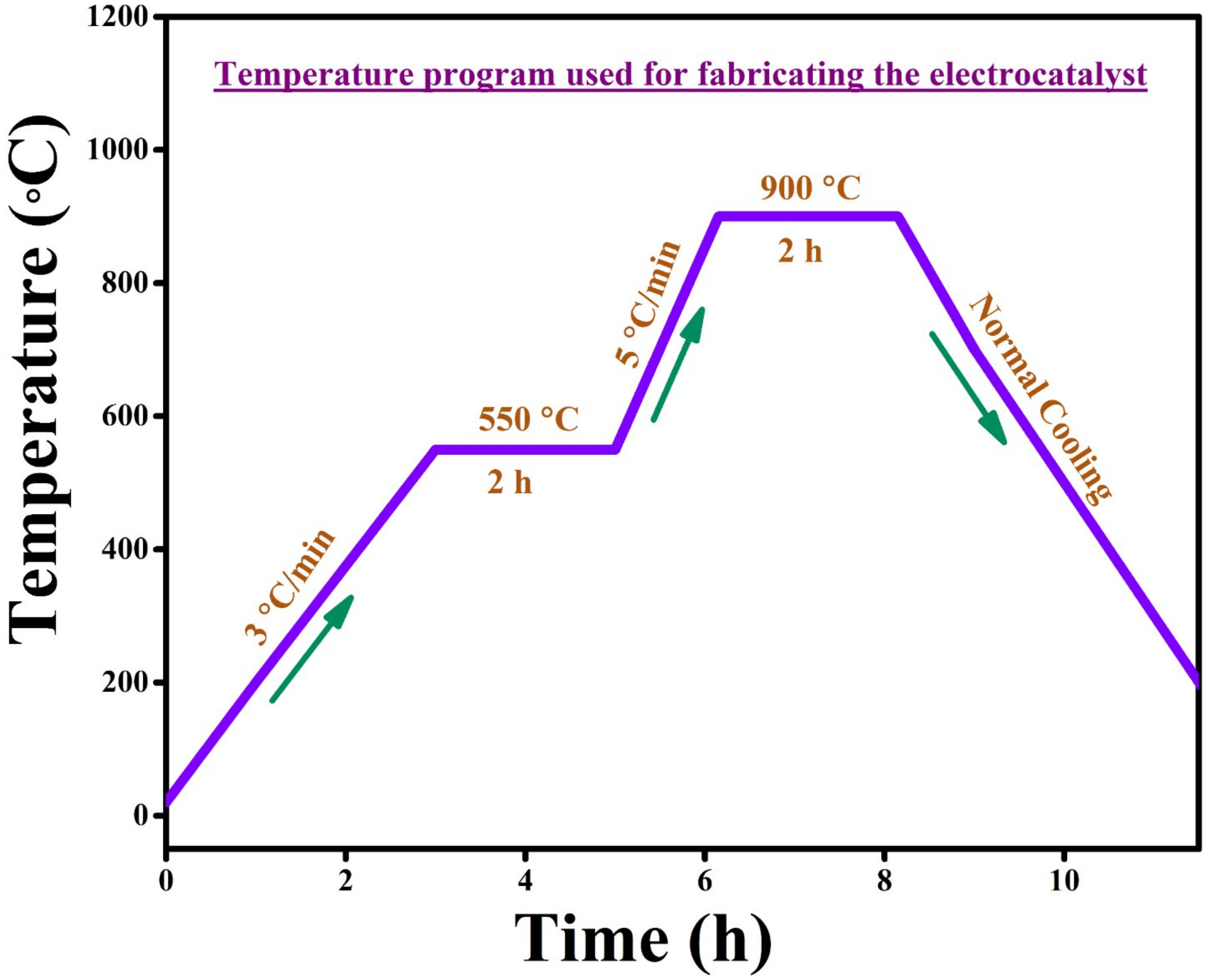

Figure S1. The temperature program applied for synthesizing the electrocatalyst.

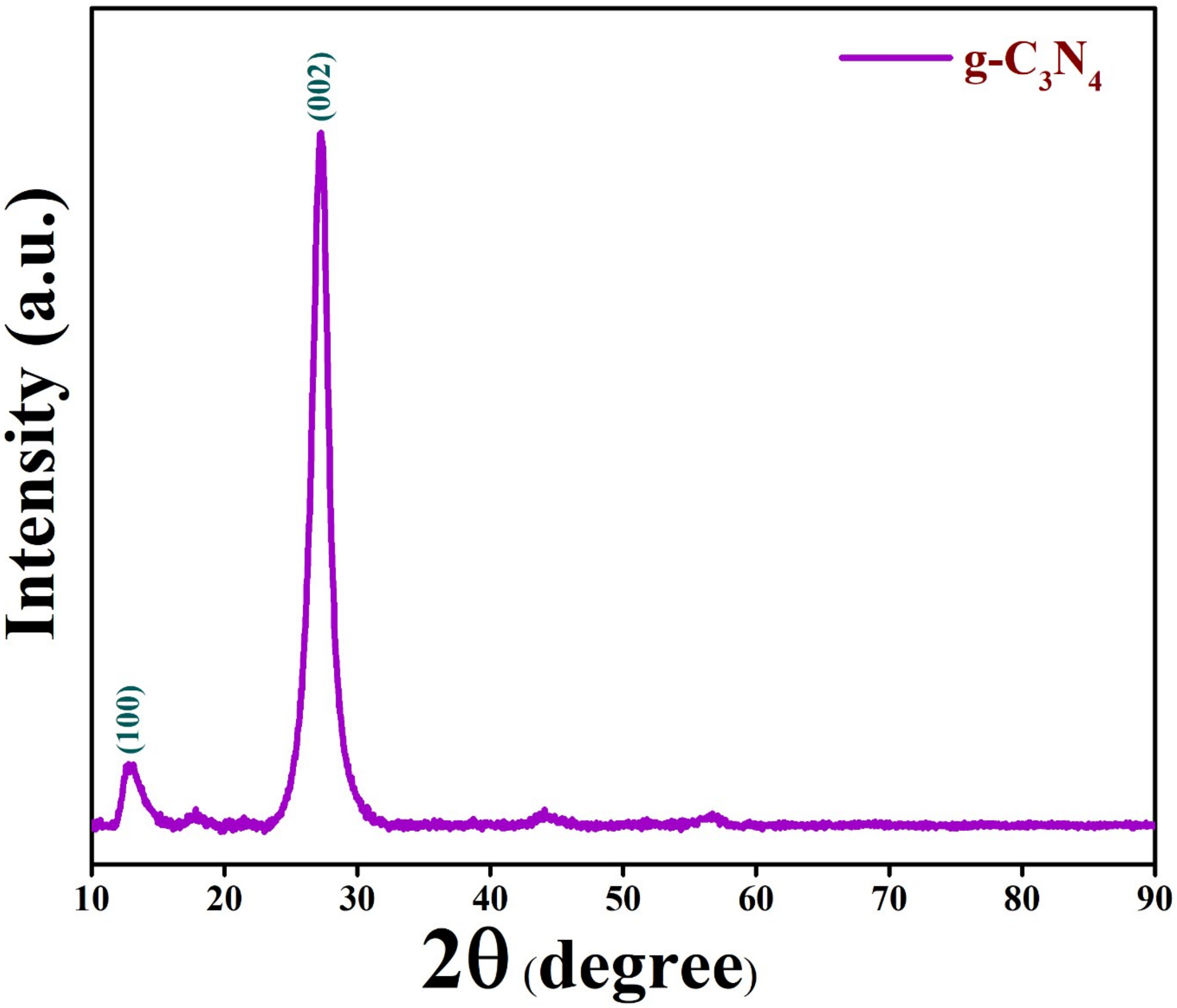

Figure S2. XRD pattern of the intermediate formed at 550 °C.

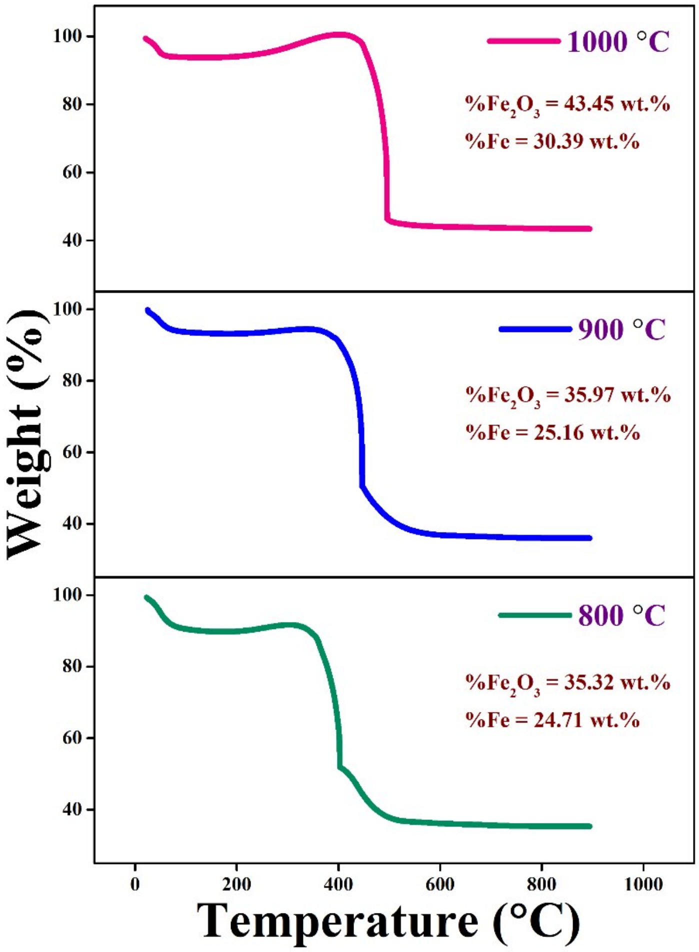

Figure S3. TGA curves under air at heating rate of 5 °C min^{-1}, for the electrocatalysts prepared at annealing temperatures of 800, 900 and 1000 °C.

Thermogravimetric analysis (TGA) for the electrocatalysts synthesized at different pyrolysis temperatures have been done under air atmosphere, to determine their total content of Fe where the temperature was ramped from room temperature to 900 °C at a heating rate of 5 °C min^{-1}. It is distinctly seen that the mass of ferric oxide (Fe_2O_3) increased from 35.32 wt.% to 43.35 wt.%, when calcination temperature was elevated from 800 to 1000 °C indicating that the relative content of Fe increased from 24.71 wt.% to 30.39 wt.%. This signifies that the weight loss diminished from 64.68 % to 56.55 %, when the reaction temperature was increased from 800 to 1000 °C. This diminution is due the more loss of carbon, nitrogen, and sulfur elements by increasing the pyrolysis temperature at which the catalyst has been synthesized, which resulted in increasing the relative content of Fe in the final material comparing to other elements. These results are well consistent with the data obtained from XRD where the calcination temperature affected the content of Fe-based nanoparticles.

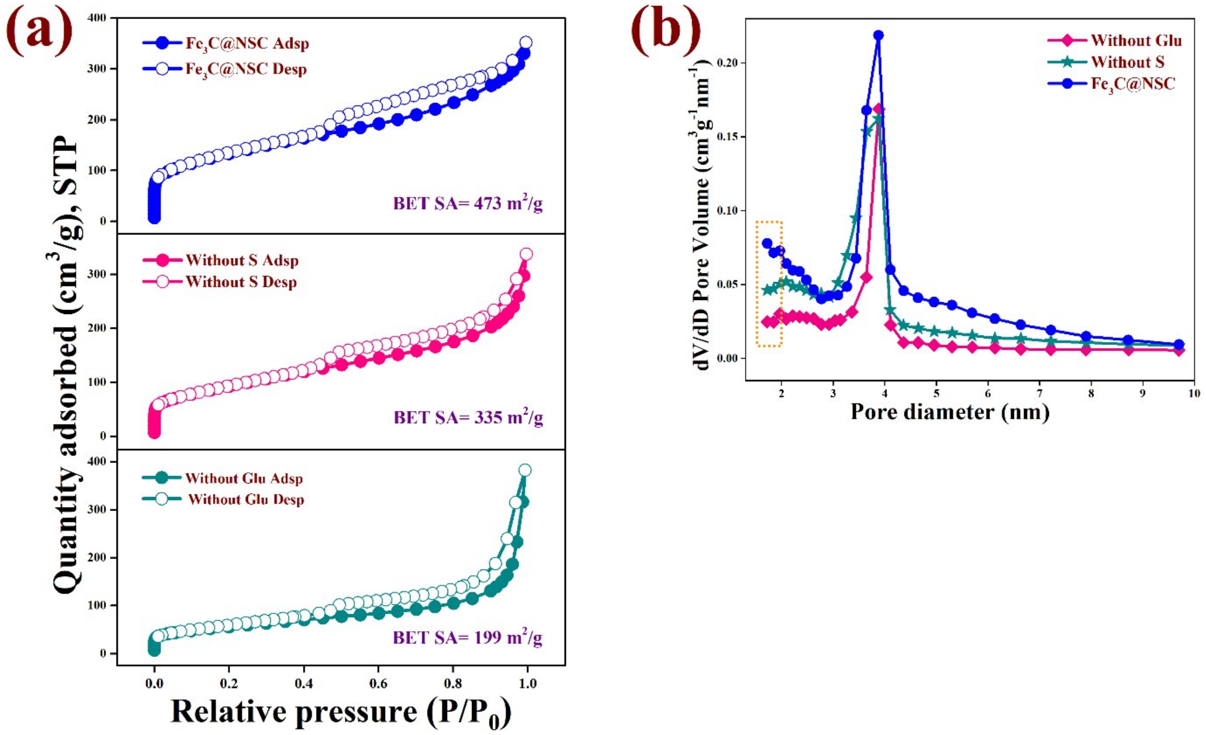

Figure S4. a) N_2 adsorption–desorption isotherms, and b) corresponding pore size distribution plots of Fe_3C@NSC/900 and the electrocatalysts synthesized without glucose or sulfur source. The dotted rectangle in b shows the comparison of the pore size distribution between the various electrocatalysts in the microporous region.

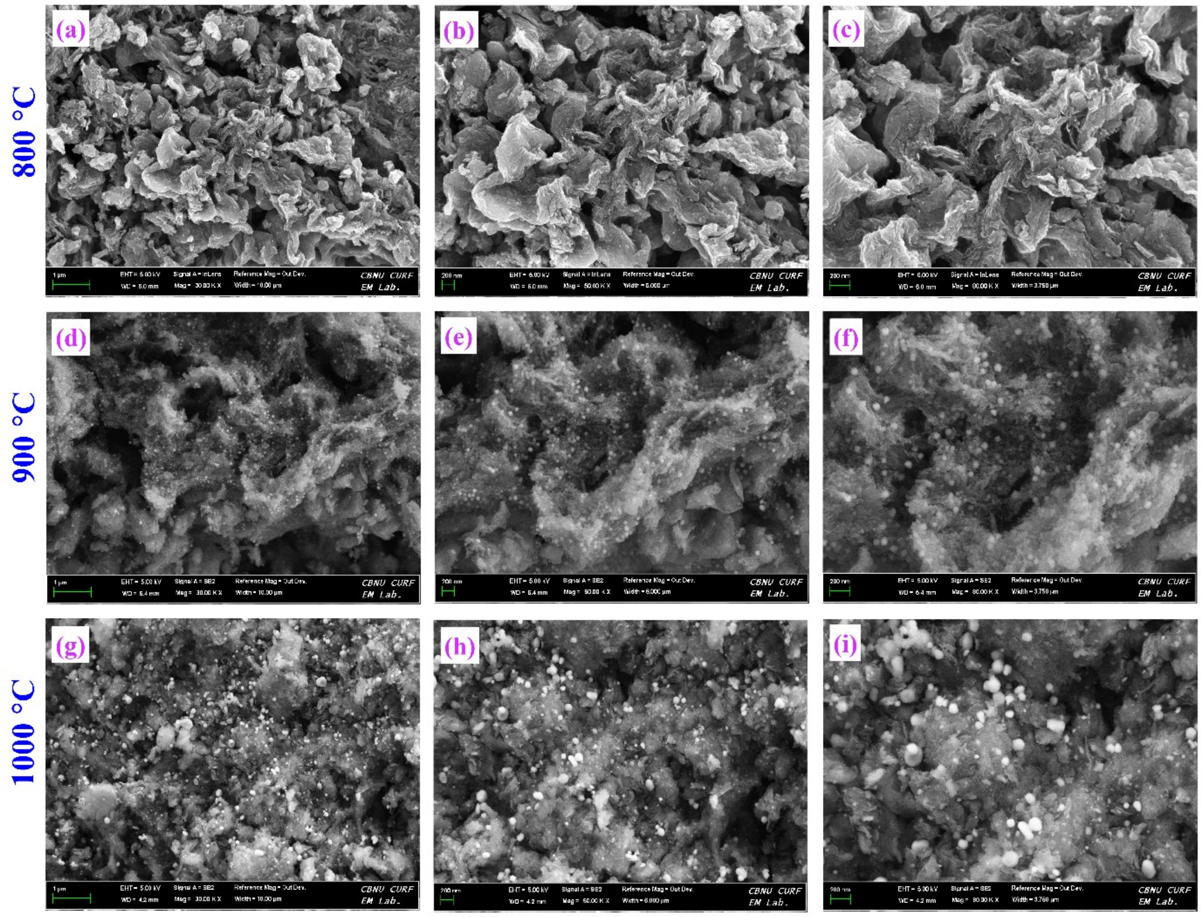

Figure S5. FESEM images at different magnifications of the Fe_3C@NSC catalysts synthesized at temperatures of 800 °C (a-c), 900 °C (d-f), and 1000 °C (g-i).

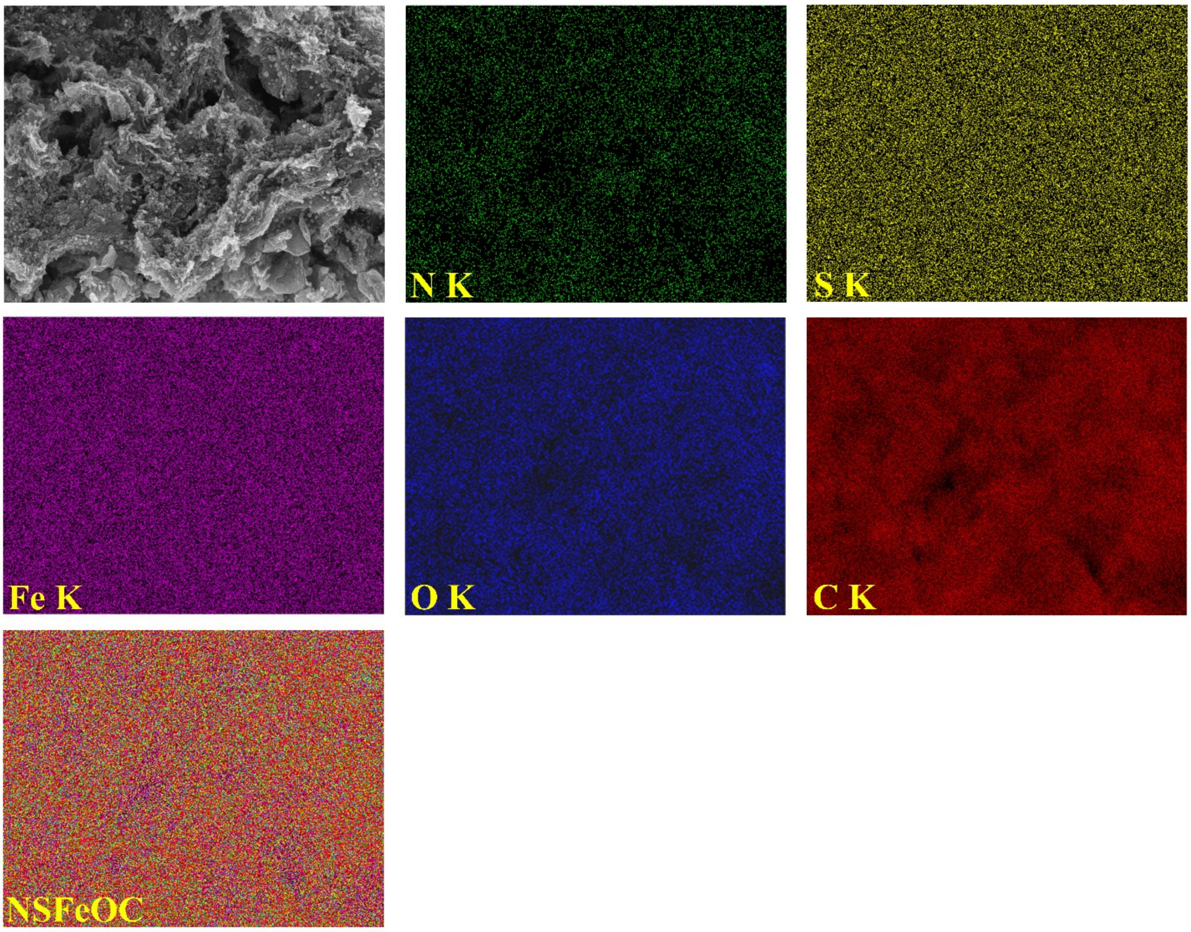

Figure S6. FESEM image and the corresponding energy dispersive X–ray spectroscopy (EDS) elemental mapping images of N, S, Fe, O, and C elements in Fe_3C@NSC/900 electrocatalyst.

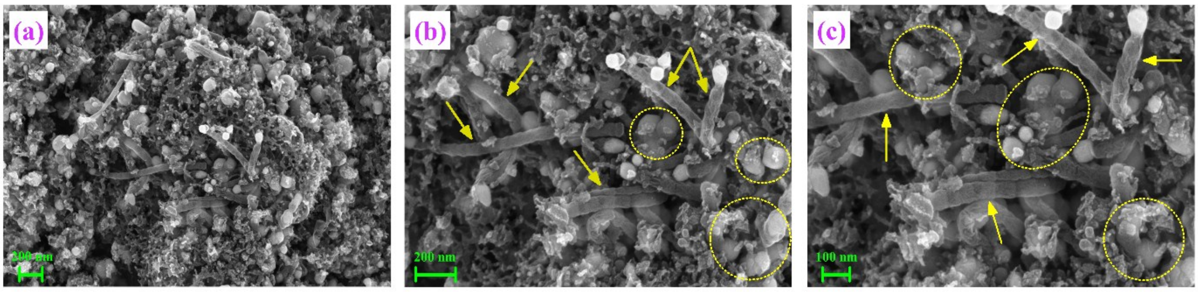

Figure S7. FESEM images at different magnifications of the electrocatalyst fabricated without glucose. The circles show the agglomeration of the nanoparticles meanwhile the arrows exhibit the formation of carbon nanotubes.

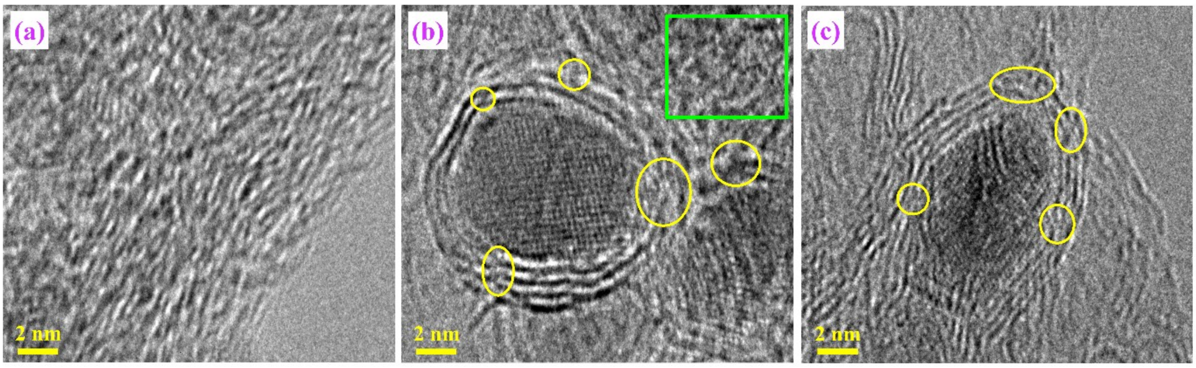

Figure S8. a) HRTEM image showing the amorphous structure of Fe_3C@NSC/900 catalyst. b, c) HRTEM images of Fe_3C@NSC/900 catalyst from various zones for a single nanoparticle. The yellow circles are exhibiting that the graphitic carbon shells are non-continuous; meanwhile, the green rectangle further exhibiting the amorphous nature of Fe_3C@NSC/900 electrocatalyst.

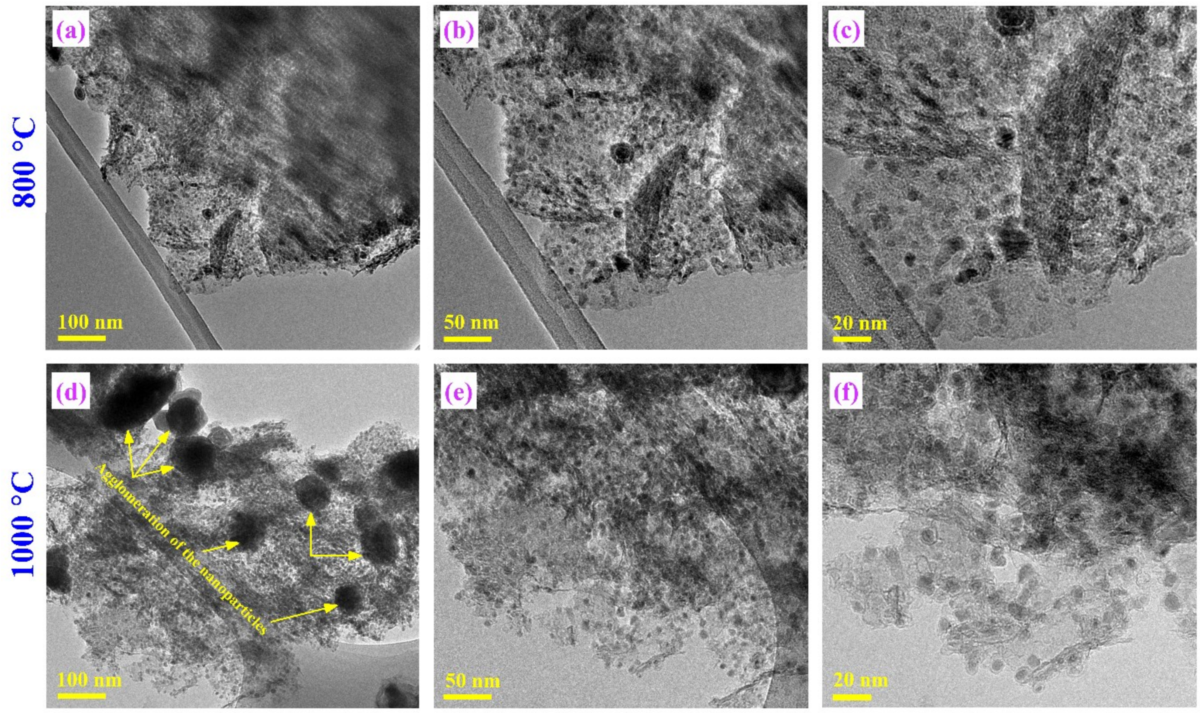

Figure S9. TEM images of Fe_3C@NSC/800 (a-c), and Fe_3C@NSC/1000 (d-f), at different magnifications. The yellow arrows in d indicate to the agglomeration of the nanoparticles.

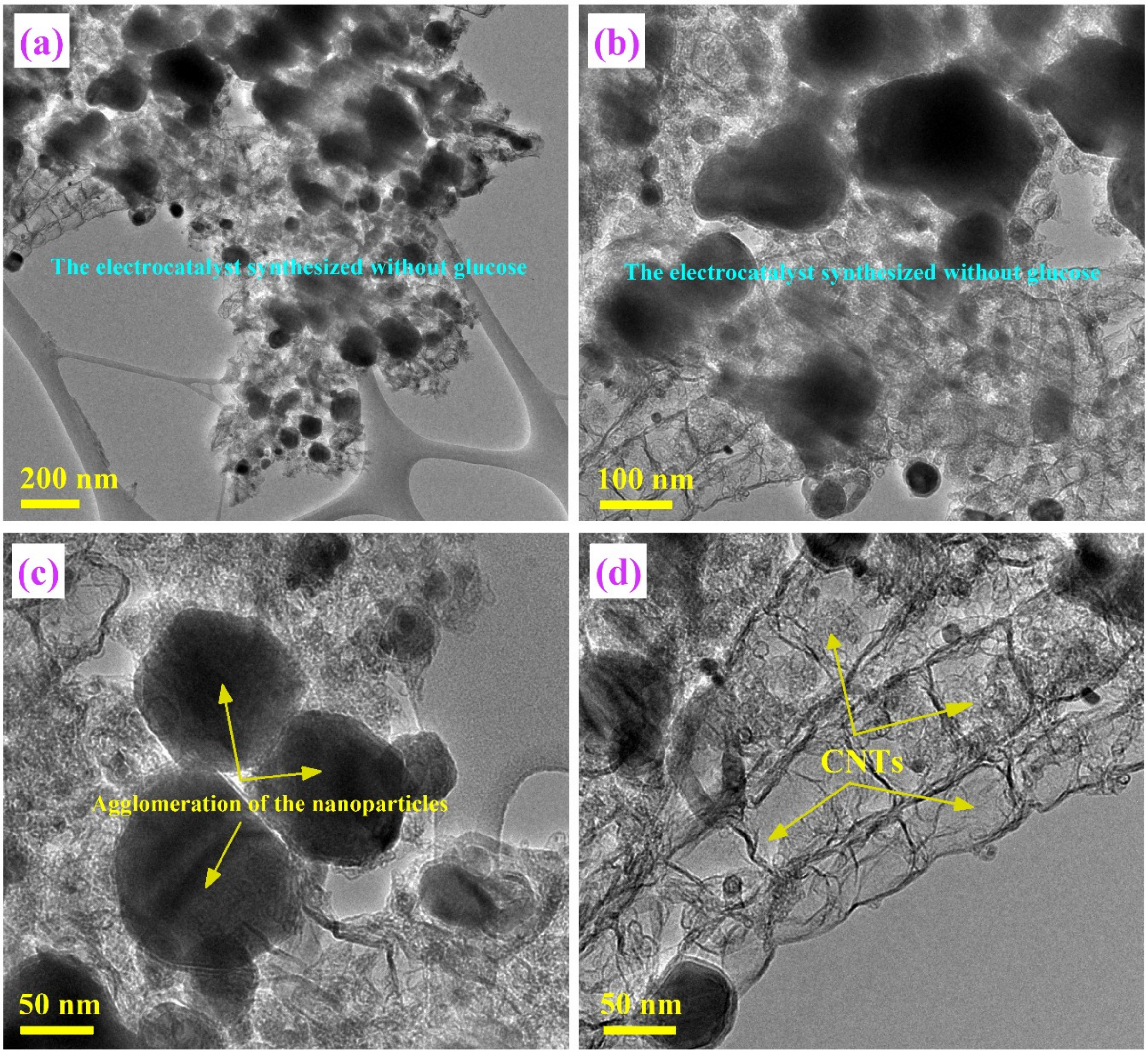

Figure S10. TEM images at different magnifications for the electrocatalyst prepared without glucose. The yellow arrows in c and d, signalize to the agglomeration of the nanoparticles and formation of carbon nanotubes, consecutively.

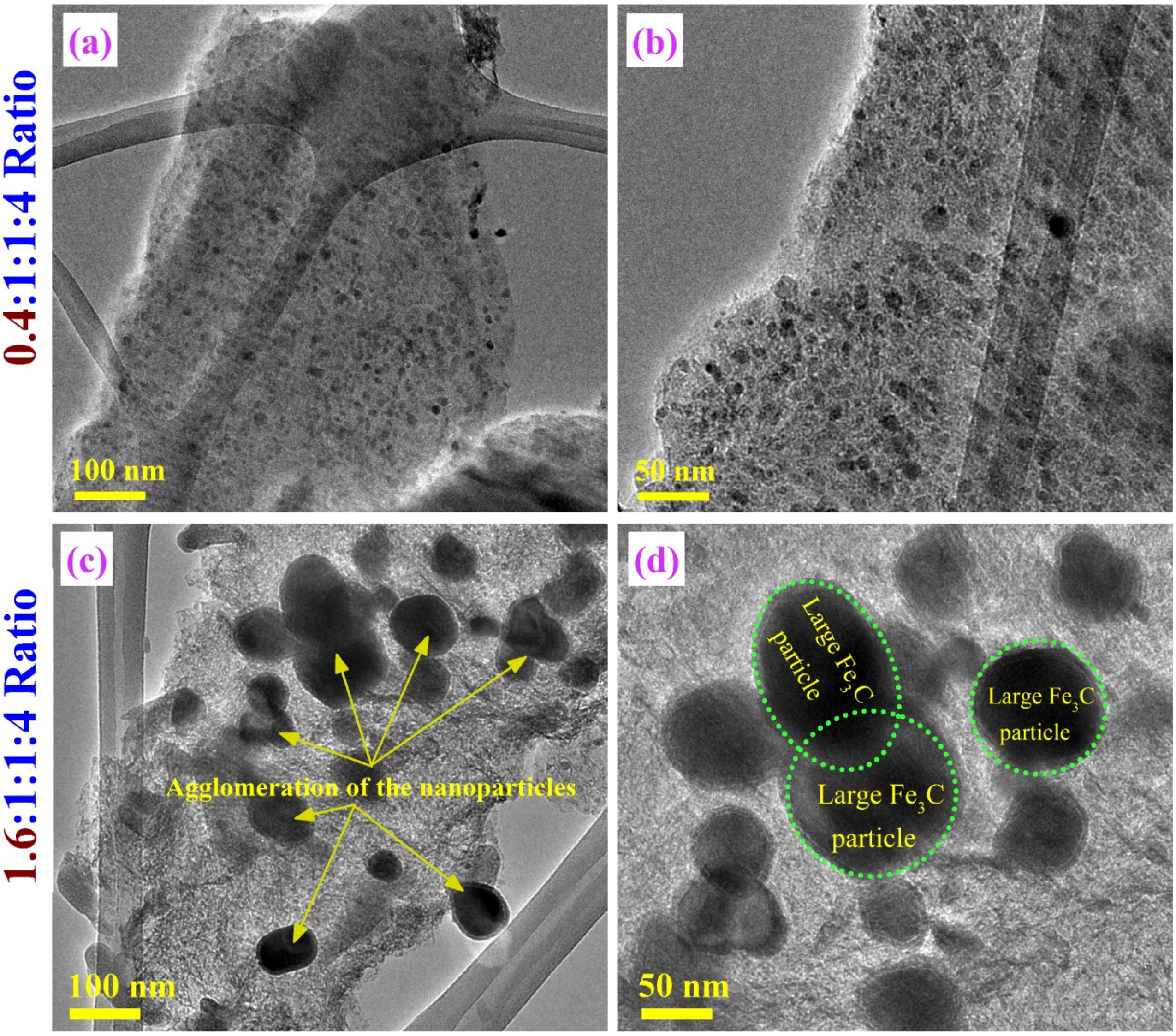

Figure S11. TEM images at different magnifications for the electrocatalyst prepared with different proportions of Fe precursor. (a and b) represent the ratio of **0.4**:1:1:4 for the precursors ($Fe(NO_3)_3.9H_2O$:CH_4N_2S:$C_6H_{12}O_6$:$C_2H_4N_4$). (c and d) represent the ratio of **1.6**:1:1:4 The yellow arrows in c and d, signalize to the agglomeration of the nanoparticles within the electrocatalyst substructure.

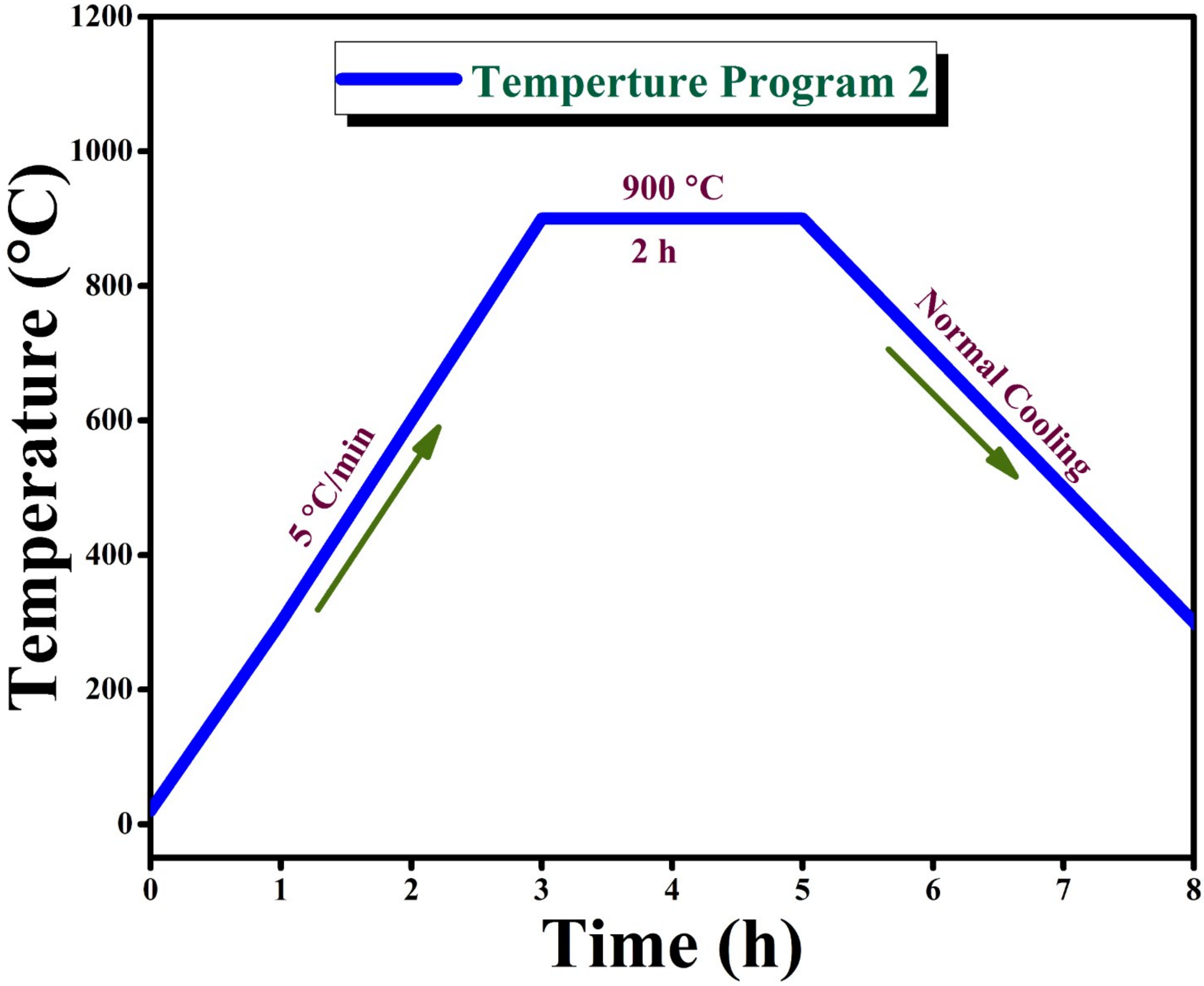

Figure S12. The second temperature program applied for synthesizing the electrocatalyst.

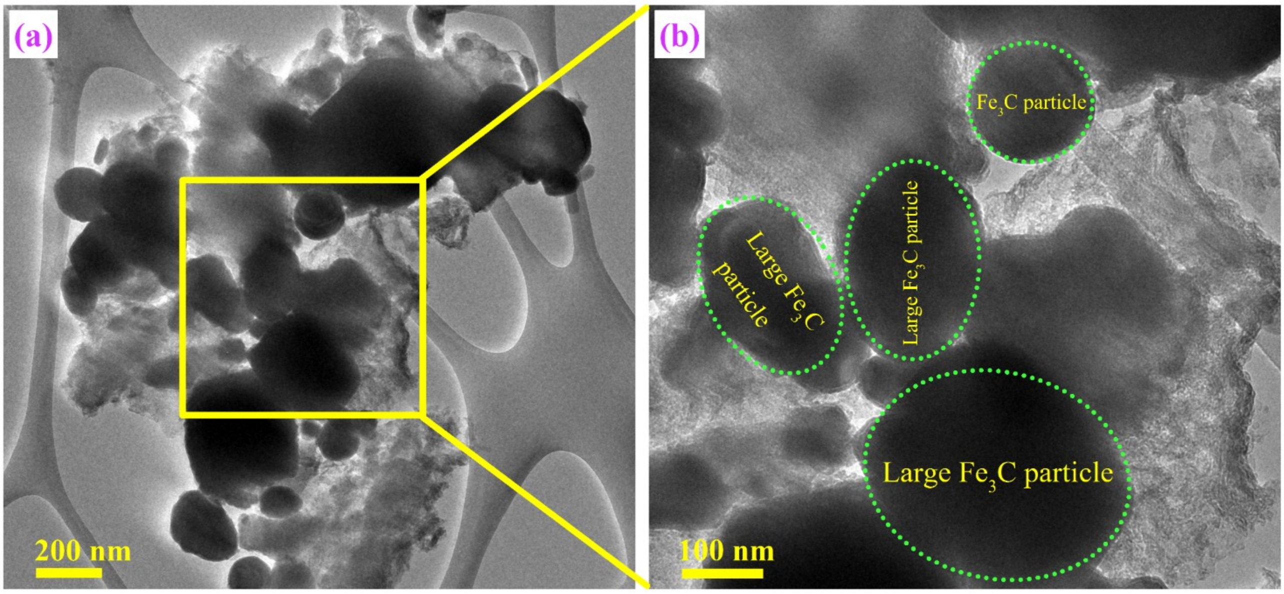

Figure S13. TEM images at different magnifications for the electrocatalyst synthesized by the reaction controlled by the second temperature program.

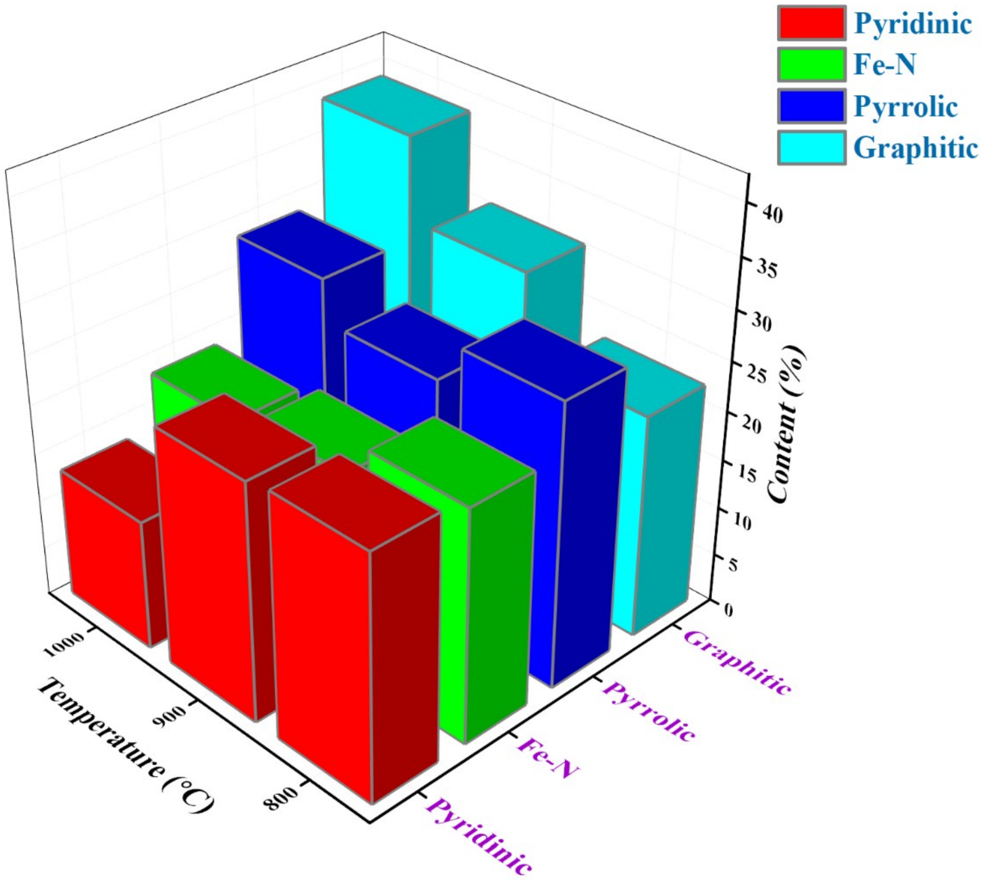

Figure S14. Contents of the different nitrogen bonding configurations in Fe_3C@NSC samples synthesized at various pyrolysis temperatures. The percentage values have been calculated by evaluating the total area of each individual peak in the deconvoluted N 1s spectra and comparing it with the total area of all peaks.

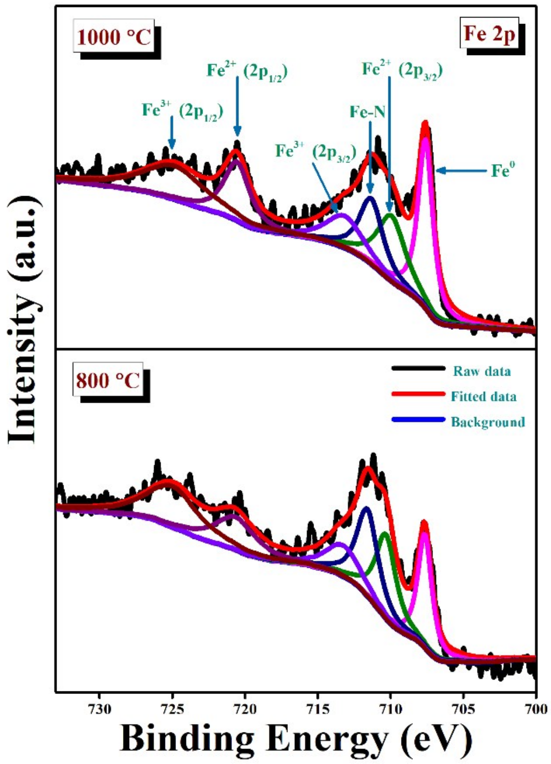

Figure S15. Fitted high-resolution XPS spectra of Fe 2p in the Fe_3C@NSC electrocatalysts prepared at temperatures of 800 °C and 1000 °C.

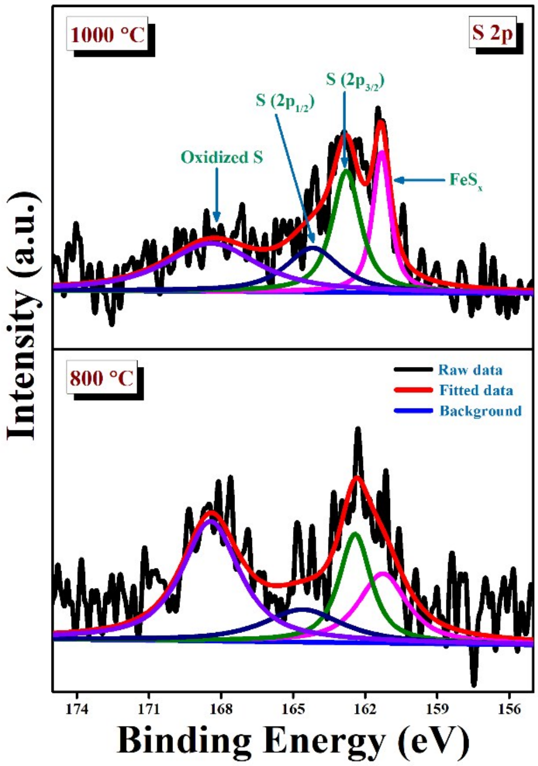

Figure S16. Deconvoluted XPS spectra of S 2p in the Fe_3C@NSC electrocatalysts synthesized at temperatures of 800 °C and 1000 °C.

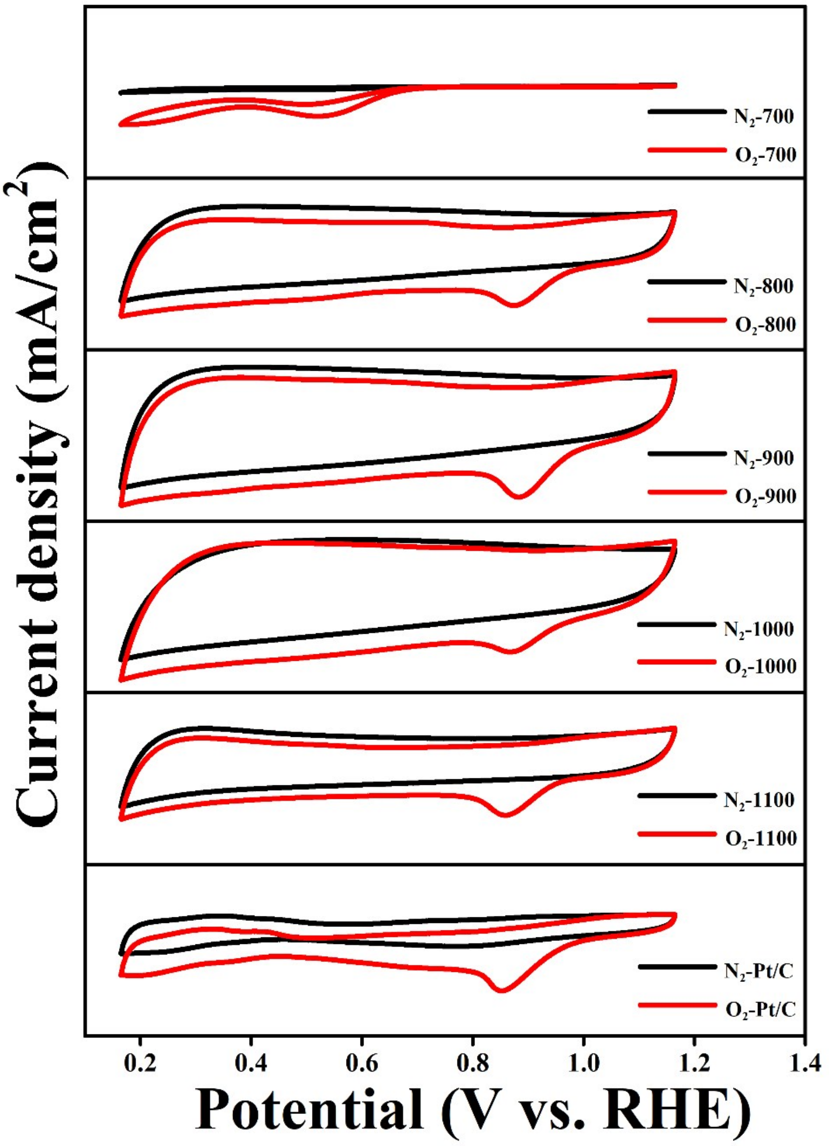

Figure S17. CV curves of Pt/C (20%), and Fe_3C@NSC synthesized at various carbonization temperatures in N_2- and O_2-saturated 0.1 M KOH solution at scan rate of 50 mV s^{-1}.

Reduction peaks were achieved by the different catalysts in O_2-saturated 0.1 M KOH solution, while no reduction peaks were observed in N_2-saturated solution indicating their electrocatalytic activity for ORR. The electrocatalyst synthesized at 900 °C showed the sharpest cathodic peak at the highest positive potential (0.889 V vs RHE), which is more positive than that of commercial Pt/C (0.856 V vs RHE) suggesting that the catalyst prepared at this temperature possessed the highest performance among all the prepared catalysts. This conclusion supports and agrees well with the results obtained from LSV technique where the effective self–doping of N, S, and Fe supply more population of active sites (Fe_3C nanoparticles, Fe–N_x sites, C–N and C–S bonds) in the carbon nanostructure of the electrocatalyst, along with a large specific surface area (473 m^2 g^{-1}), which is very beneficial for both electrocatalytic conversion and mass transport during the ORR process.

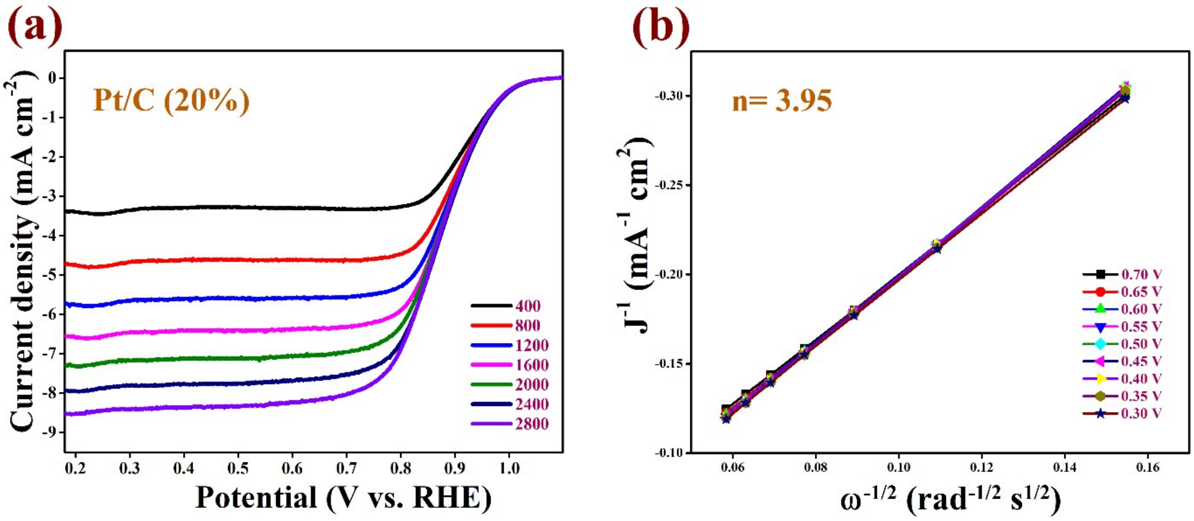

Figure S18. a) LSV curves of Pt/C (20%) at various electrode rotation rates in O_2-saturated 0.1 M KOH electrolyte and scan rate of 5 mV s^{-1}. b) Corresponding K–L plots of Pt/C (20%) at various potentials.

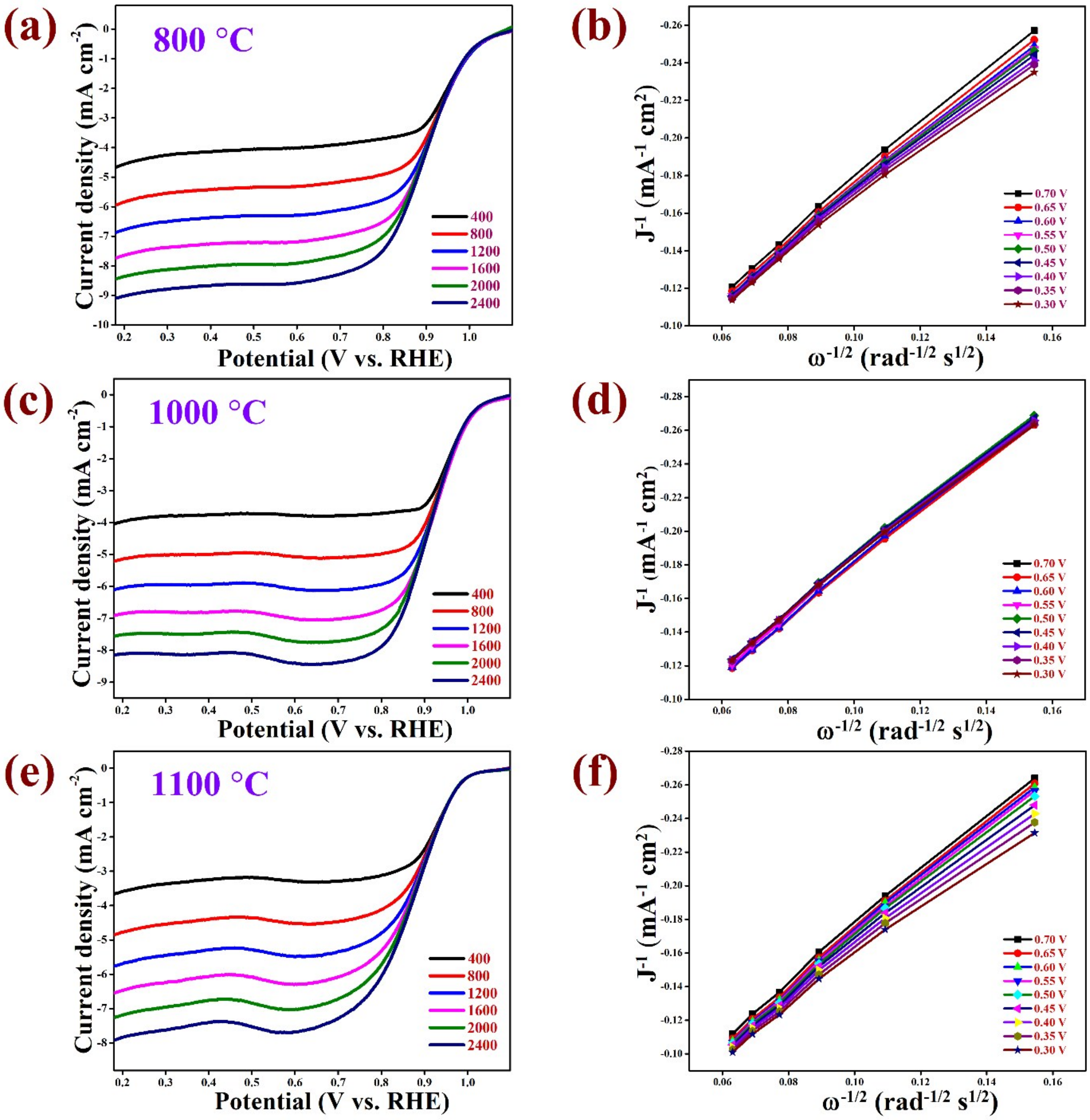

Figure S19. a, c, e) ORR polarization curves of Fe_3C@NSC catalysts pyrolyzed at different temperatures of 800, 1000, and 1100 °C, in O_2-saturated 0.1 M KOH electrolyte at scan rate of 5 mV s^{-1}. b, d, f) Corresponding K–L plots at various potentials for Fe_3C@NSC catalysts synthesized at temperatures of 800, 1000, and 1100 °C, respectively.

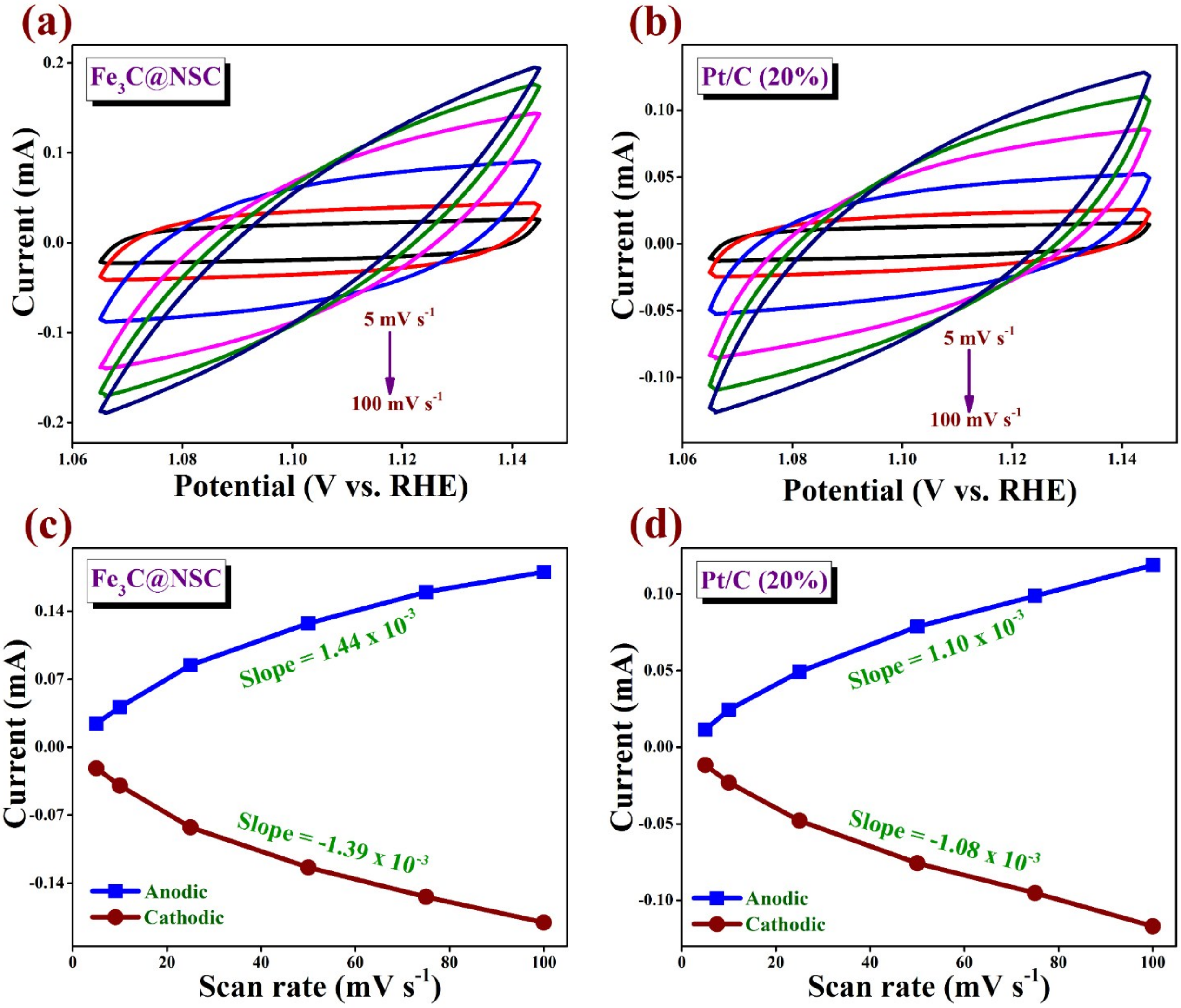

Figure S20. Capacitive cyclic voltammetry profiles of Fe_3C@NSC (a), and Pt/C (b) registered in non-Faradic region at sweep rates of 5, 10, 25, 50, 75, and 100 mV s^{-1}, in N_2-saturated 0.10 M KOH electrolyte. Anodic and cathodic currents (mA) vs scan rates (mV s^{-1}) obtained from the capacitive CV profiles of Fe_3C@NSC (c), and Pt/C (d).

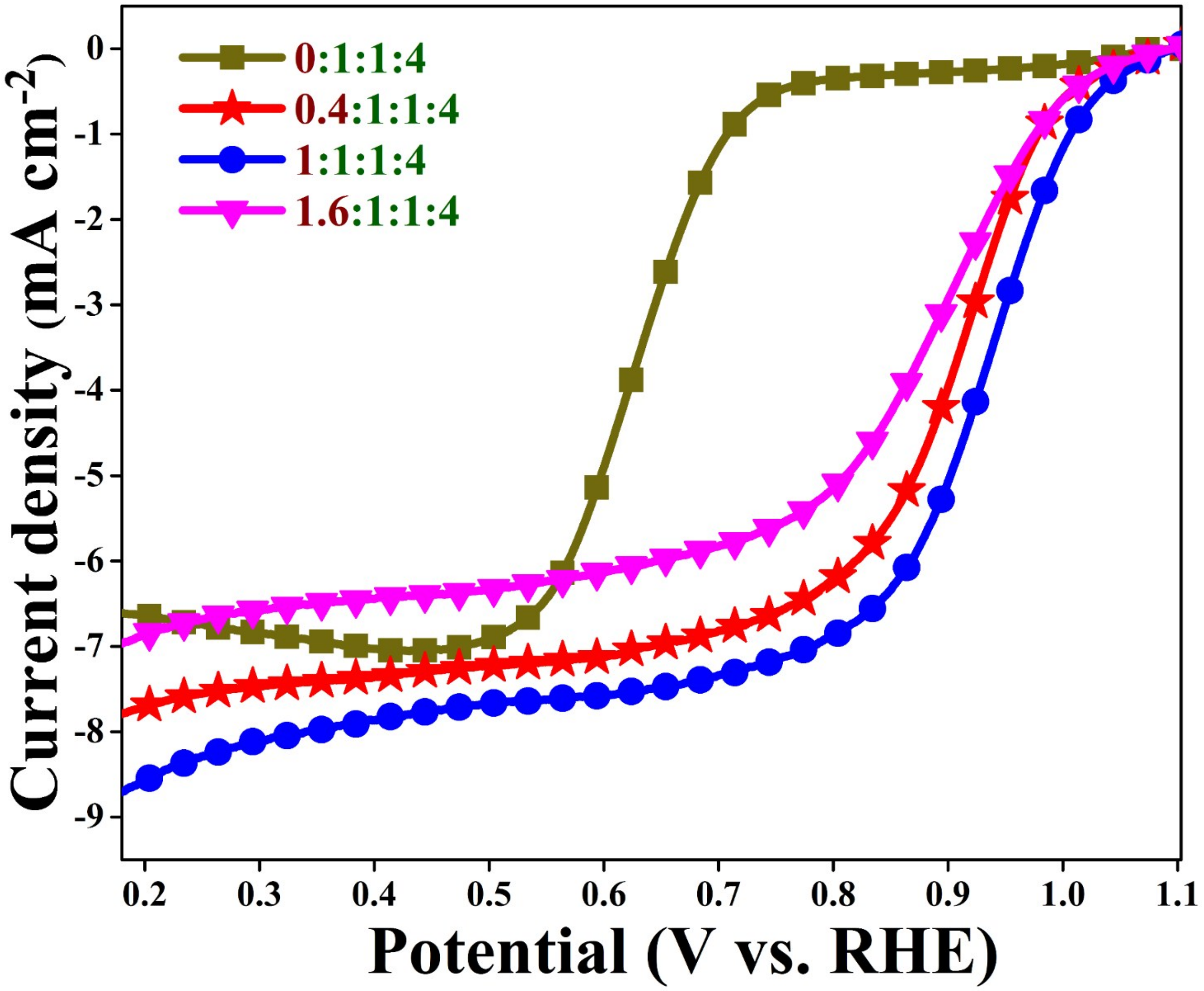

Figure S21. LSV curves of Fe_3C@NSC electrocatalysts synthesized at various ratios of Fe precursor ranging from 0 to 1.6, in O_2-saturated 0.1 M KOH electrolyte at scan rate of 5 mV s^{-1} and electrode rotation rate of 1600 rpm. The precursor ratios are in this order: $(Fe(NO_3)_3.9H_2O:CH_4N_2S:C_6H_{12}O_6:C_2H_4N_4$.

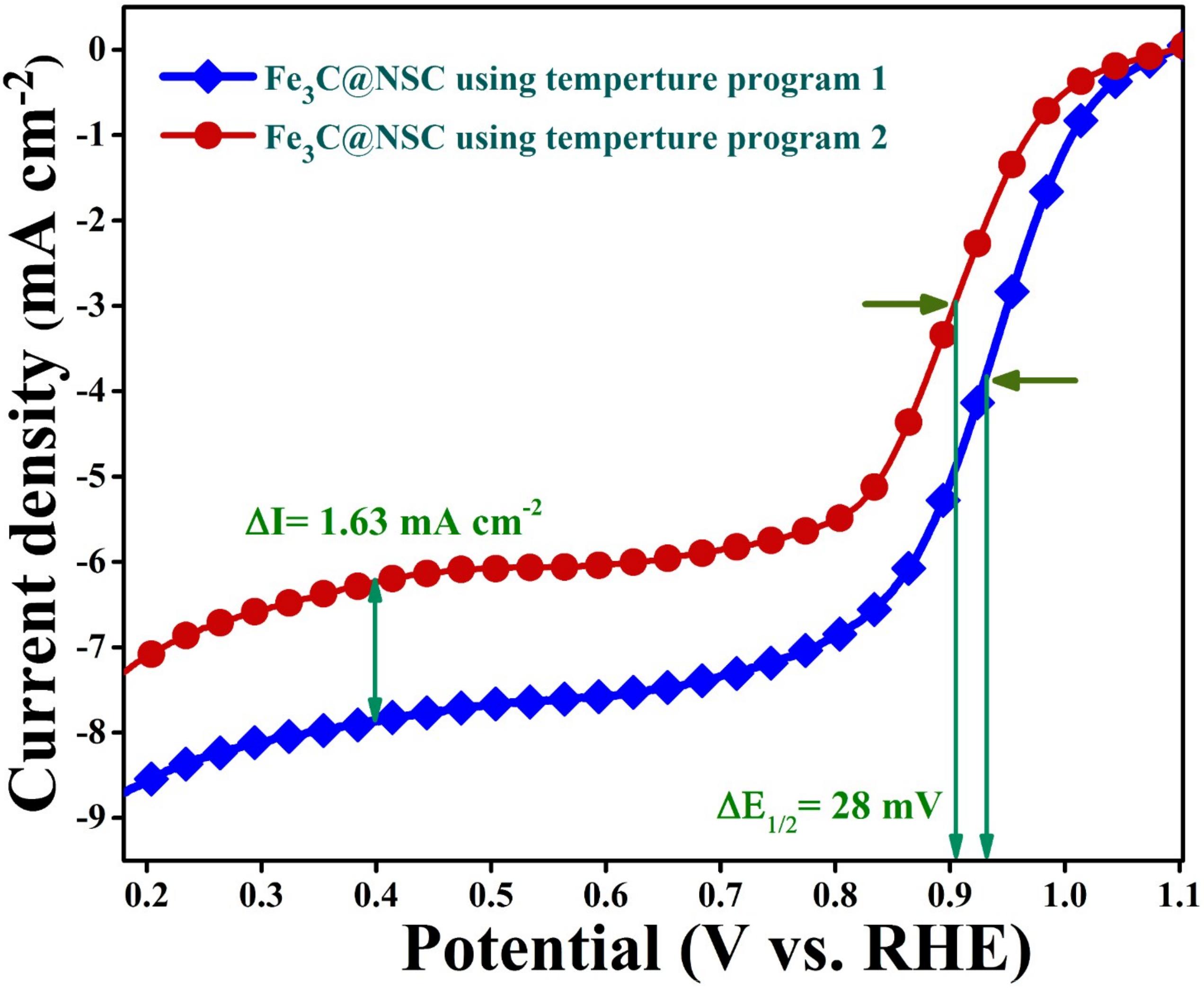

Figure S22. LSV curves of Fe_3C@NSC/900 electrocatalyst fabricated with two temperature programs, in O_2-saturated 0.1 M KOH electrolyte at scan rate of 5 mV s^{-1} and electrode rotation rate of 1600 rpm.

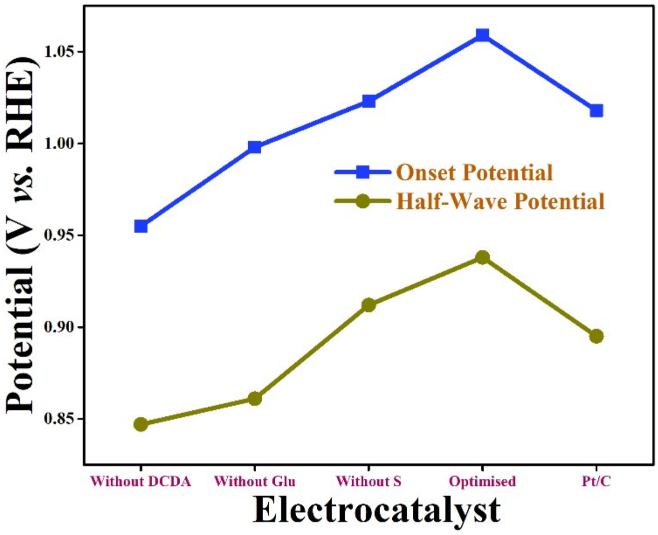

Figure S23. Relationship between the different synthesized electrocatalysts and the onset potential/half-wave potential.

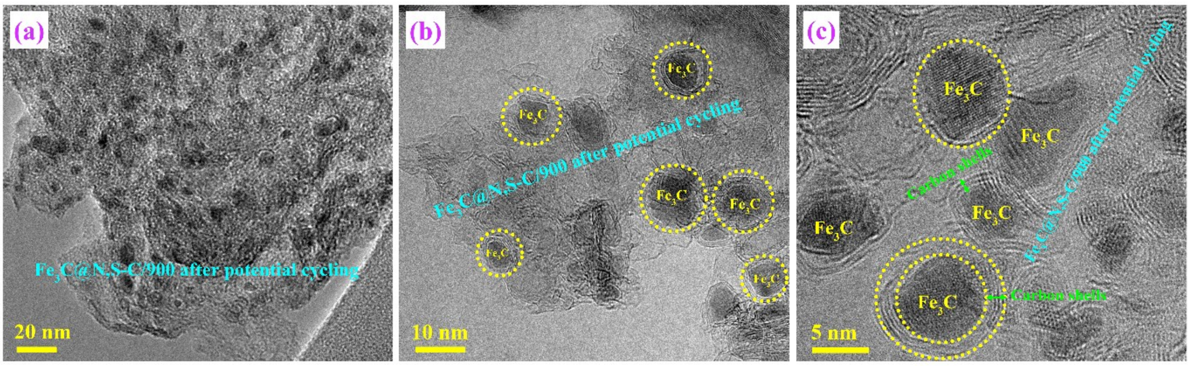

Figure S24. a, b) TEM images, and c) HRTEM image of Fe_3C@NSC/900 electrocatalyst taken after 12000 potential cycles in O_2-saturated 0.1 M KOH electrolyte. The yellow circles are showing that the electrocatalyst is still maintaining its core–shell structure even after 12000 cycles. The green arrows indicate to the carbon shells surrounding Fe_3C nanoparticles.

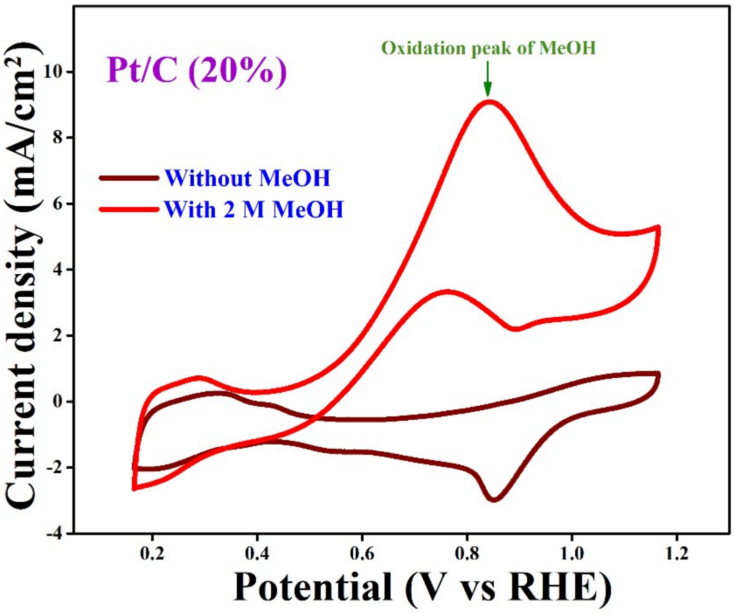

Figure S25. CV curves of Pt/C (20%) in absence and presence of 2 M methanol.

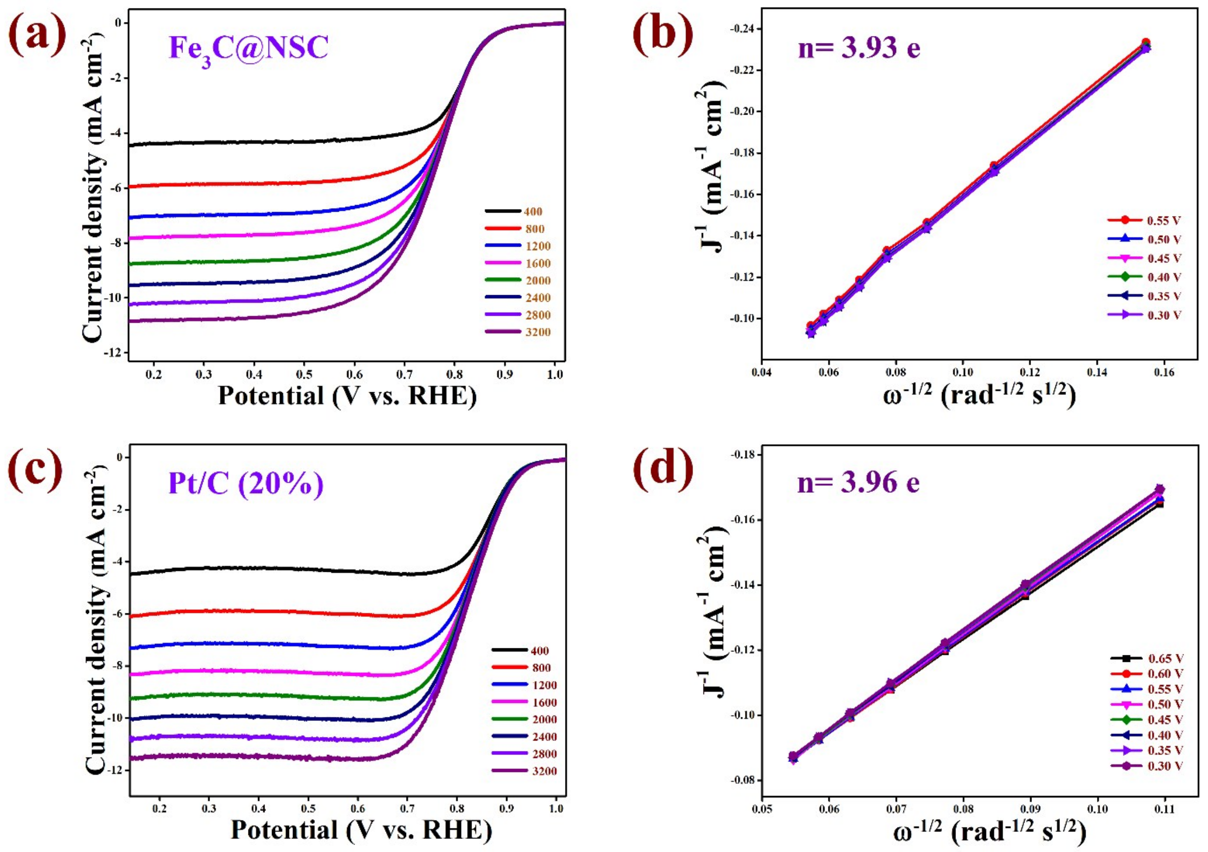

Figure S26. a, c) LSV curves of Fe_3C@NSC/900 catalyst and Pt/C (20%) at various electrode rotation speeds, in O_2-saturated 0.1 M $HClO_4$ solution at scan rate of 5 mV s^{-1}. b, d) Corresponding K–L plots at various potentials of Fe_3C@NSC/900 catalyst and Pt/C (20%).

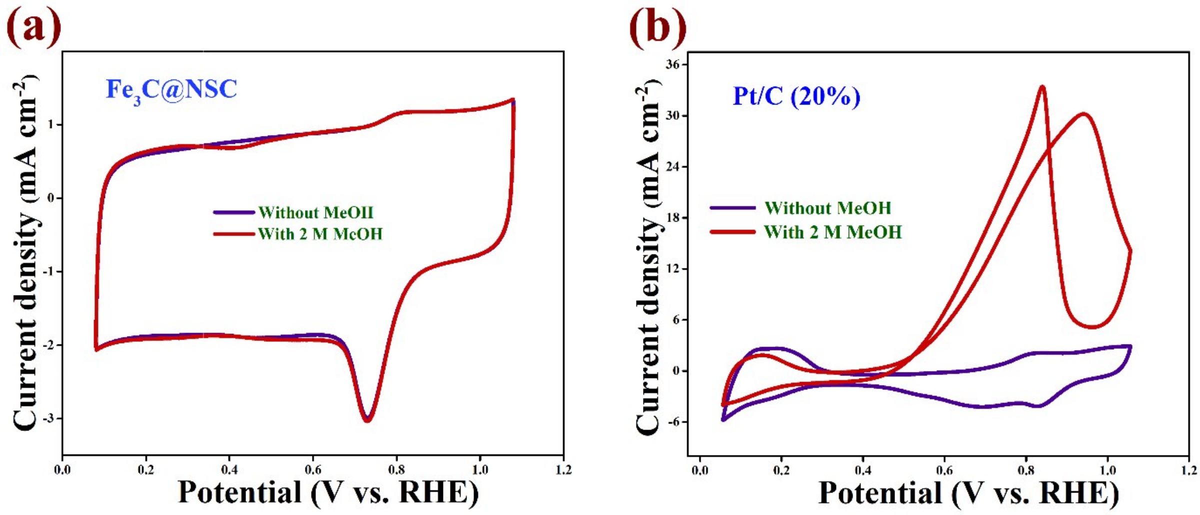

Figure S27. CV curves of Fe_3C@NSC/900 (a) and Pt/C (20%) in absence and presence of 2 M methanol in O_2-saturated 0.1 M $HClO_4$ solution at scan rate of 50 mV s^{-1}.

Table S1. Comparison of the ORR performance of reported highly efficient Fe-based electrocatalysts in the alkaline medium.

Electrocatalyst	Onset potential (V)	Half-wave potential (V)	Electron transfer Number	Reference
Fe_3C@NSC/900	**1.059**	**0.938**	**3.97**	**This work**
Pt/C (20%)	**1.018**	**0.895**	**3.95**	**This work**
GL–Fe/Fe_5C_2/NG/800	0.98	0.86	3.95–3.98	*Adv. Energy Mater.* **2018**, *8*, 1702476
$Co_{1.08}Fe_{3.34}$@NGT/750	1.03	0.94	4.08	*Adv. Energy Mater.* **2018**, *8*, 1801002
$Fe_{0.3}Co_{0.7}$/NC/800	-	0.88	3.93	*Adv. Funct. Mater.* **2018**, *28*, 1706738
Fe–ISA/SNC/900	-	0.896	3.91–3.98	*Adv. Mater.* **2018**, *30*, 1800588
Cu@Fe–N–C/900	1.01	0.892	4.0	*Adv. Funct. Mater.* **2018**, 28, 1802596
Fe_{50}–N–C-900	1.0	0.92	3.95	*Small* **2018**, *14*, 1703118
Fe_3C–Fe,N/C–900	-	0.881	3.98–4.05	*Adv. Sci.* **2018**, *5*, 1800120
pCNT@Fe@GL/950	0.911	0.811	3.96–3.99	*Adv. Mater.* **2017**, *29*, 1606534
S,N–Fe/N/C–CNT/900	-	0.85	4.0	*Angew. Chem. Int. Ed.* **2017**, 56, 610
NFe/CNs/700	0.930	0.859	3.7	*Adv. Mater.* **2017**, *29*, 1700707
Fe–N–C/900	-	0.862	3.9	*Adv. Energy Mater.* **2017**, *7*, 1701154
$Fe_{1.6}$–N–HCNS/rGO/900	-	0.872	3.98–4.02	*ACS Nano* **2018**, 12, 5674
FeBNC/800	0.968	0.838	4.0	*ACS Energy Lett.* **2018**, 3, 252
Fe@Aza–PON	-	0.839	3.7	*J. Am. Chem. Soc.*

				2018, 140, 1737
FeSAs/PTF−600	1.01	0.87	3.88	*ACS Energy Lett.* **2018**, 3, 883
Fe−CZIF−800−10	0.982	0.83	3.87−4.0	*Nanoscale*, **2018**, 10, 9252
Fe@C_2N/800	1.015	0.876	3.93.3.99	*Nano Energy,* **2018**, 44 304
Fe−N/C−950	1.04	0.895	3.92	*Nano Energy*, **2018**, 52, 29

Table S2. Comparison of the ORR performance of reported highly efficient Fe-based electrocatalysts in the acidic medium.

Electrocatalyst	Onset potential (V)	Half-wave potential (V)	Electron transfer number	Reference
Fe_3C@NSC/900	**0.924**	**0.796**	**3.93**	**This work**
Pt/C (20%)	**0.954**	**0.828**	**3.96**	**This work**
Cu@Fe–N–C/900	0.88	0.761	3.81	*Adv. Funct. Mater.* **2018**, 28, 1802596
Fe_{50}–N–C-900	0.847	-	-	*Small* **2018**, *14*, 1703118
Fe_3C-Fe,N/C-900	-	0.714	4.04–4.13	*Adv. Sci.* **2018**, *5*, 1800120
pCNT@Fe@GL/950	0.936	0.883	3.94–4.0	*Adv. Mater.* **2017**, *29*, 1606534
Fe/SNC/900	-	0.77	3.9	*Angew. Chem. Int. Ed.* **2017**, 56, 13800
Fe–C–N/950	0.95	0.81	3.99	*Adv. Mater.* **2017**, *29*, 1604556
FeSAs/PTF–600	0.89	-	3.99	*ACS Energy Lett.* **2018**, 3, 883
Fe-ZIFs/800	-	0.85	4.0	*J. Am. Chem. Soc.* **2017**, 139, 14143
p-Fe–N–CNFs	0.85	0.74	3.99	*Energy Environ. Sci.*, **2018**, 11, 2208
Fe_{14}NDC–9/900	0.821	0.73	4.0	*J. Mater. Chem. A*, **2018**, 6, 1138
Fe/N/C/900	-	0.803	3.96	*J. Mater. Chem. A*, **2018**, 6, 15504

Table S3. BET surface area (S_{BET}), microporous surface area (S_{micro}), total pore volume, and average pore size of the studied electrocatalysts.

Catalyst	**BET surface area (m^2 g^{-1})**	**Microporous surface area (m^2 g^{-1})**	**Total pore volume (cm^3 g^{-1})**	**Average pore size (nm)**
Fe_3C@NSC/800	361	18	0.375	3.88
Fe_3C@NSC/900	473	58	0.428	3.88
Fe_3C@NSC/1000	403	7	0.468	3.88
Fe_3C@NC/0%S	335	4	0.419	3.88
Fe_3C@NSC/0%Glu	199	22	0.563	3.88

Table S4. Atomic percentages of Carbon, Iron, Nitrogen, Oxygen, and Sulfur based on the XPS analysis in the electrocatalysts fabricated at different carbonization temperatures.

Sample	**C %**	**Fe %**	**N %**	**O %**	**S %**
Fe_3C@NSC/800	74.84	1.78	7.37	15.21	0.8
Fe_3C@NSC/900	83.03	1.46	5.64	9.03	0.83
Fe_3C@NSC/1000	83.37	2.24	2.9	10.76	0.73